

DOI: 10.1002/adem.201300254

Design and Fabrication of Hollow Rigid Nanolattices via Two-Photon Lithography**

By Lauren C. Montemayor, Lucas R. Meza and Julia R. Greer*

Ordered cellular solids like the octet-truss and kagome lattices have been reported to have robust mechanical properties, for example a combination of high strength and fracture toughness.^[1,2] The geometry of these structures enables creating materials with not only improved mechanical properties but also with low densities and high surface area to volume ratios. The ability to de-couple these historically coupled properties through architectural control in material design has the potential to push the envelope of existing materials in a variety of applications, from photovoltaic devices to hierarchical structural materials to materials for sustainable energy.^[3,4]

3-Dimensional structures, whose global deformation is carried out by bending of the individual struts within the structure, are often referred to as bending-dominated structures. Cellular solids whose overall deformation is carried out by stretching or compression of lattice members during loading are denoted as stretching-dominated structures. Stochastic foams with either open or closed cells represent an example of bending dominated structures whose compressive yield strength, σ_Y , has been proven to scale with the relative density, $\bar{\rho}$, as $\sigma_Y \propto 0.3\bar{\rho}^{3/2}\sigma_{YS}$ where σ_{YS} represents the yield strength of the parent solid.^[3,5] The stiffness of such structures scales as $E \propto \bar{\rho}^2 E_S$, where E_S represents the stiffness of the parent solid. An example of a stretching-dominated structure is an octet-truss lattice, shown in Figure 1c, whose strength scales with the relative density as $\sigma_Y \propto 0.3\bar{\rho}\sigma_{YS}$ and the stiffness scales as $E \propto 0.3\bar{\rho}E_S$.^[3] These scaling laws hold only for isotropic structures, i.e., whose unit cell has the anisotropy ratio, $R = 1$, defined as *width/height* of a unit cell.^[5] For isotropic geometries, stretching dominated structures have higher stiffness and strength compared to bending-dominated structures for a given relative density due to the linear relationship between relative density and both strength and

stiffness. As a result, these types of ordered cellular solids are capable of outperforming the current open-cell foams, such as stochastic metallic foams.

The relationship between fracture toughness and relative density for a 2-dimensional open-cell foam has the analytical form of $K_{IC} \propto \sigma_Y \bar{\rho}^2$ while that for a stretching dominated structure is $K_{IC} \propto \sigma_Y \bar{\rho}$.^[1] In addition to strength, the stretching dominated structures also outperform the open-cell foams in terms of fracture toughness. Another example of an ordered structure is the so-called 2-dimensional kagome lattice shown in Figure 1b, which is a stretching periodic-bending dominated structure. In 2-dimensions, the stacked triangular unit cell is a stretching dominated structure but due to the tessellation pattern, the resulting lattice has a mechanism for bending at the nodes between unit cells. As a result, the overall lattice has both stretching and bending mechanisms; hence it is called a stretching periodic-bending structure. Its fracture toughness has been reported to scale as $K_{IC} \propto \sigma_Y \bar{\rho}^{1/2}$, rendering the kagome lattices to be tougher than the stretching and bending dominated geometries for low relative densities.^[1] The higher fracture toughness offered by the kagome lattice in 2-dimensions, compared to other lattice geometries, make it is reasonable to expect similar advantages in a 3-dimensional kagome geometries. Evans et al.^[6] have created a macro-scale version of the 3-dimensional kagome lattice but the structure was limited to a single unit cell in height. The 3-dimensional kagome unit cell presented in this paper can be tessellated to create lattices of multiple unit cells in height, thus providing a platform to fully study the mechanical behavior of the kagome lattice in 3-dimensions. If the high fracture toughness properties of the 2-dimensional geometry extend to the 3-dimensional kagome lattice, it will allow for the creation of nanostructured materials with the ability to inhibit crack propagation and increase damage tolerance of a structure for a given constituent material.^[1,2]

Ultra-lightweight small-scale hollow cellular structures have been fabricated using photolithographic techniques.^[4,7–10] In contrast to traditional photolithography techniques, which typically produce 2-dimensional structures, Jacobsen et al.^[9] created 3-dimensional structures by exposing a bulk volume of photoresist to collimated ultra-violet (UV) light through a mask. In their process, a 3D polymer waveguide was formed during exposure as a result of the change in index of refraction between the cured and uncured photoresist. The 3-dimensional geometry created by the polymer waveguide is fully defined by the lithographic mask pattern and by the

[*] Prof. J. R. Greer, L. C. Montemayor, L. R. Meza
1200 E. California Blvd MC 309-81, Pasadena, CA 91125, USA
E-mail: jrgreer@caltech.edu

[**] The authors gratefully acknowledge the financial support from the Dow-Resnick Innovation Fund at Caltech and from the National Science Foundation through L.C.M.'s NSF Graduate Research Fellowship and J.R.G.'s grant (CMMI-1234364). The authors acknowledge critical support and infrastructure provided by the Kavli Nanoscience Institute at Caltech. The authors would also like to thank Dongchan Jang for assistance in TEM sample preparation and analysis.

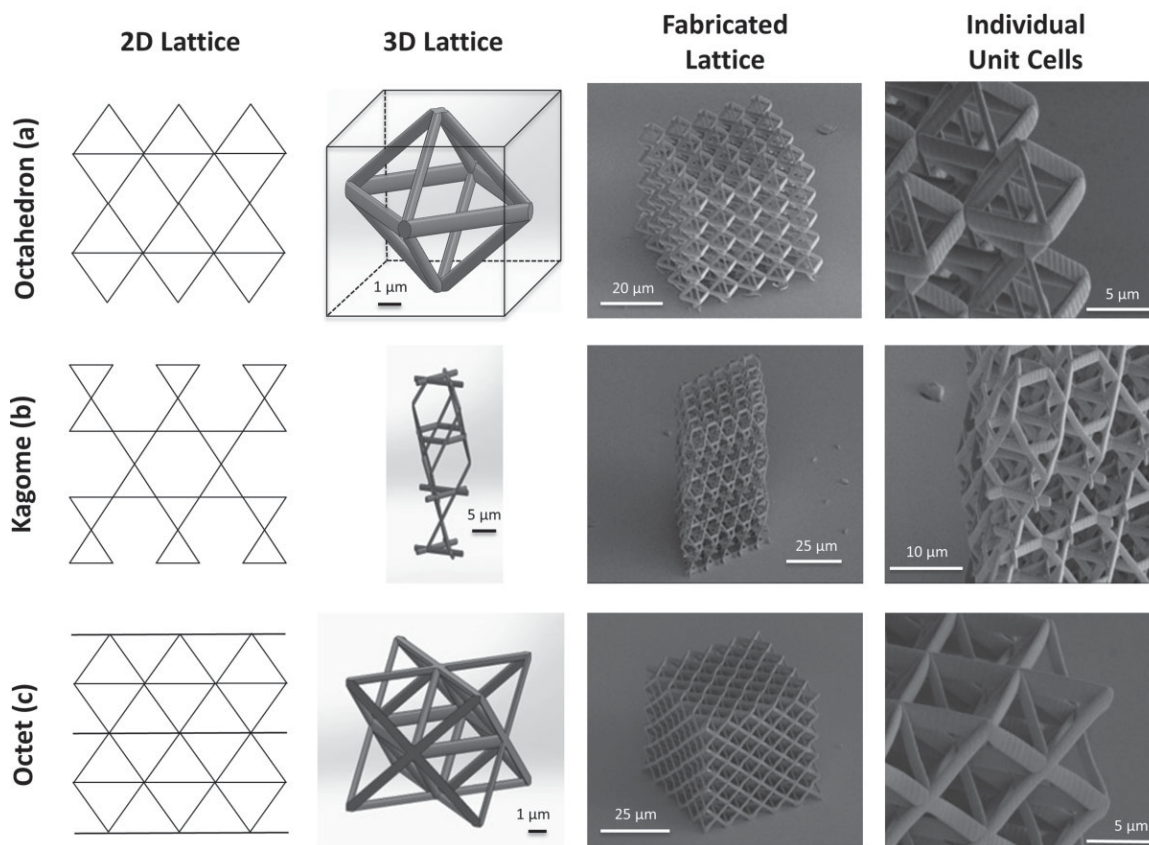


Fig. 1. CAD model and SEM images of fabricated structures for three different nanolattice geometries: octahedron (a), kagome (b), and octet (c). The fabricated structures closely match the design at each relevant scale. The 3D octahedron (a) demonstrates the volumes used to calculate relative density, as detailed in the Section 1 (image tilt of 55°–60°).

interactions of the light beams passing through the individual apertures. In this process, the light must pass within some constrained angle of vertical through the mask to provide the energy necessary to create the polymer waveguide, which limits the applicability of this process to create only specific geometries. For example, such single exposure mask photolithography technique cannot be used to create horizontal lattice members. As a result, photolithography does not allow complete control over the geometry of 3-dimensional architectures.

Rapid prototyping techniques used to create 3-dimensional structures, such as 3D printing (3DP), allow complete control over the geometry of a structure. 3DP is a relatively time-consuming additive fabrication process in which a structure is formed by a rastering process that deposits adhesion or bulk material to create thin cross-sectional layers.^[11] The process begins at the base and builds up in cross-sectional increments, which adhere together, until the structure is complete. This technique has been used to fabricate scaffolds that are similar to ordered cellular solids, with the dimensions on the order of hundreds of microns and larger.^[12,13] Current 3DP technology has a layer resolution of approximately 100 μm, a lateral resolution of 40 μm, and an estimated write speed of 7 μm s⁻¹.^[11,14] The ultimate resolution for 3DP is limited to approximately 200,000 elements/mm³ while rapid

prototyping techniques utilizing a laser curing process are predicted to have an ultimate resolution on the order of 13 000 000 elements/mm³ and an improved surface roughness of the fabricated structure.^[15]

With the advance in technologies such as two-photon direct laser writing lithography (TPL), it has become possible to create 3-dimensional geometries with features ranging from millimeters to nanometers in size.^[16–20] In contrast to single exposure photolithographic techniques, TPL allows full control of the geometry of a structure in 3-dimensions, similar to 3DP, but with improved resolution. Similar to the structures produced by 3DP and optical photolithography techniques, geometries created using TPL are polymer based and fabrication methods need to be developed to create structures on this length scale with other types of materials. TPL combines the advantages of 3D printing and photolithography to provide full control in creating small-scale structures on a variety of length scales with a resolution down to 150 nm.^[19,20]

This work describes the fabrication of hollow metallic nanolattices with dimensions spanning from 100 nm to 1 μm to 10 μm and larger. The two-photon lithography fabrication process shown in Figure 2 was used to create the 3-dimensional structures that were designed using SolidWorks, a computer aided design (CAD) program, as shown in Figure 2a. The design was then imported as a set of points describing the

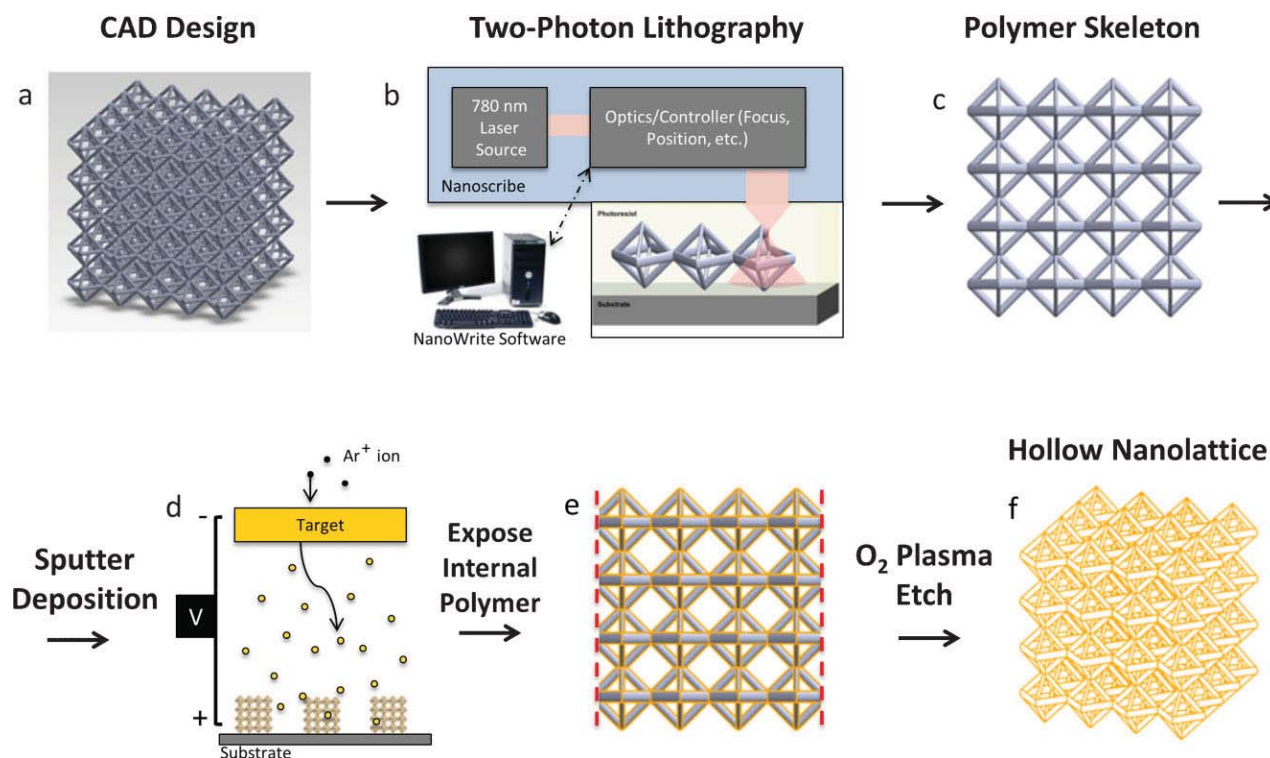


Fig. 2. Process flow to create hollow rigid nanolattices. A 3-dimensional structure is first designed using CAD software (a) and then replicated into a polymer pattern using two-photon lithography (b). After development, the polymer structure (c) is conformally coated with a thin metallic layer via sputtering (d). The edges are removed using a focused ion beam to uncap polymer within each strut (e), and the entire polymer skeleton is removed using an oxygen plasma etch revealing a hollow, rigid nanolattice (f).

vertices of the unit cell, which defines the structure, to NanoWrite, a program that interfaces with the Nanoscribe TPL instrument to write the designed structure in a polymer. The unit cell was then patterned to create nanolattice arrays that were $5 \times 5 \times 3$ –5 unit cells large, depending on the geometry, to make structures with dimensions of approximately $50 \mu\text{m} \times 50 \mu\text{m} \times 50 \mu\text{m}$. Once the structure was defined and imported into the NanoWrite Software, the IP-Dip photoresist, specially design by Nanoscribe GmbH to optimize the TPL process, was exposed to a 780 nm femtosecond pulsed laser. The laser was focused to a region denoted as the voxel, which is elliptically shaped with an aspect ratio of 3.8 and has sufficient energy to initiate cross-linking of the photoresist to create the polymer structure.^[21] The voxel was traced in 3-dimensions according to the points defining the structure by a piezoelectric motor, with a resolution of $\pm 10 \text{ nm}$ and a maximum displacement of $300 \mu\text{m}$. By altering the power of the laser and the speed with which the voxel moves through the photoresist, the size of the voxel and the exposure of the photoresist can be controlled to create features as small as 150 nm .^[19,20]

A parameter matrix varying the laser power and writing speed was explored to determine the optimal parameters for creating structurally stable arrays. When the laser power/write speeds were too low, the structures collapsed under capillary forces during the development process. On the opposite end of the spectrum, when the laser power/write speeds were too high, certain regions within the photoresist experienced very high-energy concentrations, which led to

small-scale explosions and destroyed the structures. The laser power was varied from 8 to 12 mW and the writing speed varied from 45 to $70 \mu\text{m s}^{-1}$. For nano-lattices of the size described in this paper, the optimal parameters were found to be a laser power of 10 mW and a write speed of $45 \mu\text{m s}^{-1}$. After exposing the photoresist, the structures were developed for 30 min in propylene glycol mono-methyl ether acetate (PGMEA) followed by a 3-min rinse in isopropyl alcohol. Once the polymer nanolattice was isolated, it was then coated using sputter deposition, as shown in Figure 2c and d. To demonstrate the fabrication process, gold was used to sputter coat the polymer nanolattices. The conformality of the gold coating depends on the pressure, power, and deposition time during the sputtering process. Various pressures, powers, and times were investigated to determine the optimal sputtering parameters. For gold, the optimal parameters were found to be at a working pressure of 5 mTorr and a power of 50 W for a carrier gas of argon flowing at 10 sccm. The gold was sputtered for 60 min under these conditions resulting in a gold layer of approximately 90 nm on the nanolattice surface. As shown in Figure 1, the fabricated structures after sputtering deposition closely matched the computer designed structures on all relevant length scales for three different nanolattice geometries. After the polymer lattices were coated in gold, this initial scaffold was removed to reveal hollow metallic nanolattices. To remove the polymer, the structure was exposed to an oxygen plasma treatment at a pressure of 1 Torr and flow of 300 sccm O_2 for 2 h. The nanolattices were milled on two sides with a

focused ion beam (FIB) at a current density of 7 nA to expose the polymer so the oxygen plasma could penetrate inside the scaffold and etch away the polymer. Gold was chosen as the model sputtering material primarily because it does not react with the oxygen plasma required to remove the polymer, though it is a representative material and any material resistant to oxygen plasma that can be sputtered can be used for this fabrication process. As shown in Figure 2e and f, the remaining structure after the FIB/etch process described above is a hollow, rigid nanolattice.

After the process shown in Figure 2, the fabricated structures were sliced 1/3, 1/2, and/or 2/3 along the depth of the lattice using the FIB, with the conditions described above, and then visually inspected to assess the conformality of the gold coating. Figure 3 shows representative cuts through various types of structures and verifies the conformality of the coating through the depth of the nanolattice. By analyzing the cross-sectional thickness of the hollow nanolattice members, it was verified that the approximate thickness of the gold coating, under the optimal sputtering conditions described above, was 90 ± 30 nm. The coating thickness was averaged over 20–50 thickness measurements at various lattice depths and locations for each of the octahedron, kagome, and octet nanolattice geometries.

In addition to the sputtering conditions, the relative density of the polymer structure plays a role in the degree of metallic film uniformity. A solid rather than a hollow nanolattice was

used to calculate the relative density because it is the diffusion of the sputtered material into the polymer structure that creates a conformal coating on the nanolattice. The relative density of a nanolattice depends both on the geometry and size of the unit cell and the calculation is described in detail in the Section 1. The calculated relative densities for the various geometries are shown in Figure 4. Both the octahedron and octet unit cells can be contained in a $10 \mu\text{m} \times 10 \mu\text{m} \times 10 \mu\text{m}$ unit cell volume since the angle between non-perpendicular members is defined to be 45° . For a unit cell volume of $10 \mu\text{m} \times 10 \mu\text{m} \times 10 \mu\text{m}$, the octahedron has a relative density of 0.040 and the octet structure has a higher relative density of 0.077 due to additional members in the unit cell. Figure 4 shows that the sputtering process did not coat the octet nanolattice conformally at relative densities higher than approximately 0.040. When the unit cell dimensions of the octet structure increased from $10 \mu\text{m} \times 10 \mu\text{m} \times 10 \mu\text{m}$ to $15 \mu\text{m} \times 15 \mu\text{m} \times 15 \mu\text{m}$, the relative density became 0.036 and the structure could be conformally coated with the sputtering conditions described above. For a kagome lattice with a similar relative density of 0.031, the gold coating was also found to be conformal. Figure 4 shows three lattice geometries that can be coated conformally using sputter deposition, though for structures with relative densities higher than approximately 0.040, the coating began to lose integrity.

We present a methodology to create 3-dimensional hollow metallic hierarchical structures with length scales spanning

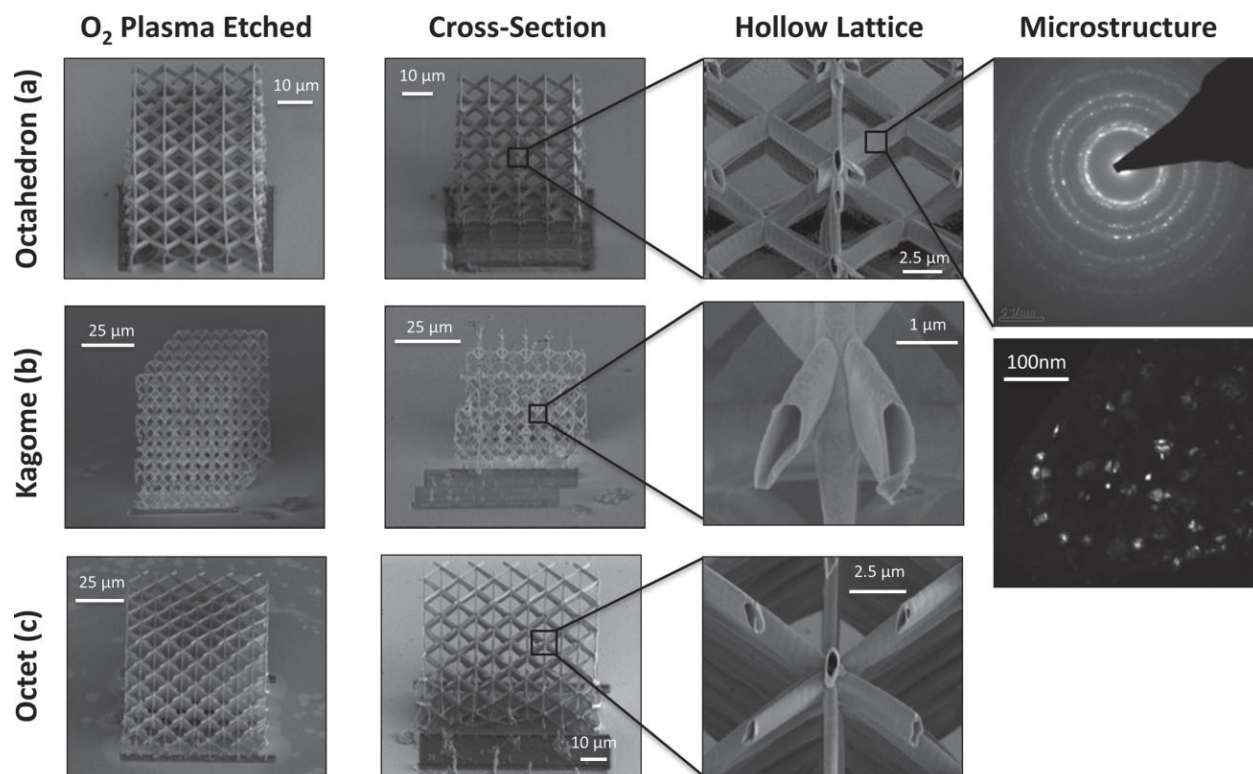


Fig. 3. SEM images of the hollow structures for the three lattice geometries: octahedron (a), kagome (b), and octet (c) after sputtering and etching steps as shown in Figure 1 (image tilt of 52°). Representative transmission electron microscopy (TEM) dark-field image of an octahedron lattice member showing the nanocrystalline structure of the sputtered coating with grain size on the order of 20–50 nm.

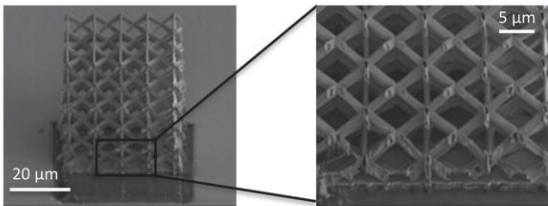
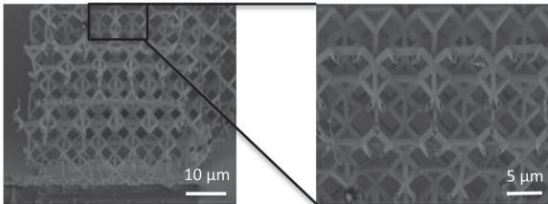
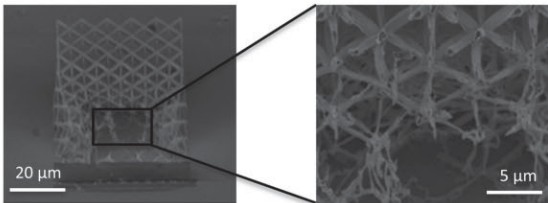
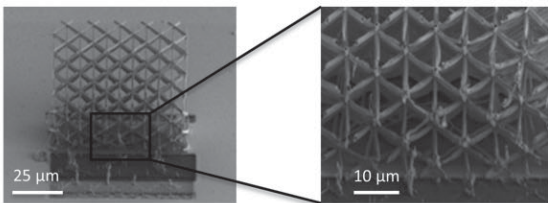
		Relative Density $\bar{\rho} = \rho_{\text{structure}} / \rho_{\text{solid}}$	Surface Area:Volume $SA_{\text{structure}} / V_{\text{solid}}$
Octahedron (a)		0.40	$5.96 \mu\text{m}^{-1}$
Kagome (b)		0.031	$6.60 \mu\text{m}^{-1}$
Octet (c1) (c2)		0.077	$7.73 \mu\text{m}^{-1}$
		0.036	$7.84 \mu\text{m}^{-1}$

Fig. 4. SEM images of representative nanolattices for different relative densities and geometries: for relative densities ≈ 0.040 , the octahedron (a), kagome (b), and octet (c2) structures coat conformally under optimal sputtering conditions. For higher relative densities, such as octet (c1), the sputtering is not conformal throughout the structure. Note the high surface area to volume ratio for each of the nanolattice structures, making these structures ideal for solar/fuel cell applications.

from $50 \mu\text{m}$ to hundreds of nanometers generated using a two-photon lithography technique. The ability to fabricate structures not limited by geometry with higher resolution than previous technologies provides an opportunity to engineer structures at many length scales. Ultra-lightweight, low-density structures can now be engineered and fabricated with this methodology to outperform those that currently exist, such as stochastic foams, by controlling the lattice geometry. Not only can the deformation mechanism of the structure on the macro-scale be controlled through the geometry, thus potentially increasing its strength and fracture toughness, but its hierarchical nature also provides opportunities to harness the “smaller is stronger” size effect that has been observed in metals on the nanoscale.^[22,23] This size effect has previously been observed in nano-pillars but the ability to potentially harness this effect in a more structurally robust system allows for the size effect to be utilized in a variety of applications. The fabrication process demonstrated in this paper presents a way to create a structure with potential to capitalize on the combined effects of lattice geometry and size-induced material properties with potential applications ranging from bio-compatible structural materials to fuel and solar cells.

1. Experimental

1.1. Speed Exposure Matrix

The laser power and write speed conditions for the TPL process were varied to determine the correct exposure of the photoresist to create structures. For low exposures, the structures would collapse during the development process. For high exposures, the photoresist would explode and the structure would be destroyed. Laser power was varied from 8 to 12 mW in increments of approximately 0.67 mW and the speed was varied from 45 to $70 \mu\text{m s}^{-1}$ in increments of $4.17 \mu\text{m s}^{-1}$ for the octet structure. This produced an exposure matrix covering six laser powers and six write speeds, for a total of 36 different exposures. The best structures were produced for photoresist exposure with speeds between 45 – $50 \mu\text{m s}^{-1}$ and laser powers of 8.8 – 11.2 mW and the optimal conditions were chosen to be at $45 \mu\text{m s}^{-1}$ and 10 mW for the structures shown in this paper.

1.2. Sputtering Conditions

Gold was chosen as the sputtering material due to its resistance to oxidation that is required for the oxygen plasma etching to remove the internal polymer, however this

fabrication technique is applicable for any oxidation resistant material that can be sputtered. A DC power source was used for the sputtering process and initial parameters of 100 W and a working pressure of 3 mTorr with argon at 10 sccm was tested. For a 30-min deposition time, the structures did not coat conformally so the time was increased to 60 min. After 60 min of gold deposition at these parameters, the structures appeared to have a more conformal coating. To improve the coating, powers of 100 and 50 W and pressures of 3 and 5 mTorr were tried, resulting in a total of four sputtering conditions, keeping the sputtering time constant at 60 min and the carrier gas as argon at 10 sccm. For conditions of 100 W and 5 mTorr, the coating was very flaky and did not adhere well to the structure or substrate. The most conformal coating for the octet, octahedron, and kagome structures was found to be at 50 W and 5 mTorr.

1.3. Relative Density Calculation

The relative density of the structures was calculated by considering the volume fraction of the structure, which is equivalent to the density of the cellular structure over the bulk density for a given material.^[24] The conformality of the coating depended on the relative density of the structure on which is being coated. In this case, the relative density of the solid member polymer structure is the density that must be considered. To calculate the volume of the polymer structure, a SolidWorks model of the unit cell was used. Dimensions of the structure in SolidWorks were set using the measured dimensions of the polymer structured based on SEM images. Using these dimensions, the volume of the polymer unit cell contained in the unit cell was calculated using the SolidWorks model. The volume fraction was found by dividing the volume of the polymer structure contained in the unit cell by the volume of the unit cell, demonstrated in Figure 1a for the octahedron structure, which is equivalent to the relative density of the structure. A single unit cell was considered in this calculation since the volume of the structure and the bulk both scale by the number of units cells that form the lattice.

Received: July 12, 2013

Final Version: September 3, 2013

[1] N. A. Fleck, X. Qiu, *J. Mech. Phys. Solids* **2007**, 55, 3.

- [2] V. S. Deshpande, N. A. Fleck, M. F. Ashby, *J. Mech. Phys. Solids* **2001**, 49, 8.
- [3] N. A. Fleck, V. S. Deshpande, M. F. Ashby, *Proc. R. Soc. A* **2010**, 466, 2121.
- [4] L. Valdevit, A. J. Jacobsen, J. R. Greer, W. B. Carter, *J. Am. Ceram. Soc.* **2011**, 94, S1.
- [5] L. J. Gibson, M. F. Ashby, in *Cellular Solids: Structure and Properties*, Cambridge University Press, Cambridge, UK **1999**.
- [6] J. Wang, A. G. Evans, K. Dharmasena, H. N. G. Wadley, *Int. J. Solids Struct.* **2003**, 40, 25.
- [7] T. A. Schaedler, A. J. Jacobsen, A. Torrents, A. E. Sorensen, J. Lian, J. R. Greer, L. Valdevit, W. B. Carter, *Science* **2011**, 334, 6058.
- [8] A. Torrents, T. A. Schaedler, W. B. Carter, L. Valdevit, *Acta Mater.* **2012**, 60, 8.
- [9] A. J. Jacobsen, W. Barvosa-Carter, S. Nutt, *Acta Mater.* **2008**, 56, 11.
- [10] A. J. Jacobsen, W. Barvosa-Carter, S. Nutt, *Adv. Mater.* **2007**, 19, 22.
- [11] D. T. Pham, R. S. Gault, *Int. J. Mach. Tools Manuf.* **1998**, 38, 10.
- [12] W.-Y. Yeong, C.-K. Chua, K.-F. Leong, M. Chandrasekaran, *Trends Biotechnol.* **2004**, 22, 12.
- [13] C. X. Lam, X. Mo, S. Teoh, D. Hutmacher, *Mater. Sci. Eng. C* **2002**, 20, 1.
- [14] H. G. Lemu, *AIP Conf. Proc.* **2012**, 857, 1.
- [15] C. K. Chua, S. M. Chou, T. S. Wong, *Int. J. Adv. Manuf. Technol.* **1998**, 14, 2.
- [16] C. N. LaFratta, J. T. Fourkas, T. Baldacchini, R. Farrer, *Angew. Chem. Int. Ed.* **2007**, 46, 33.
- [17] J. Fischer, M. Wegener, *Laser Photon. Rev.* **2013**, 7, 1.
- [18] H. B. Sun, S. Kawata, *Adv. Polym. Sci.* **2004**, 170, 169.
- [19] W. Xiong, Y. S. Zhou, X. N. He, Y. Gao, M. Mahjouri-Samani, L. Jiang, T. Baldacchini, Y. F. Lu, *Light: Sci. Appl.* **2012**, 1, 4.
- [20] N. Tétreault, G. von Freymann, M. Deubel, M. Hermatschweiler, F. Pérez-Willard, S. John, M. Wegener, G. Ozin, *Adv. Mater.* **2006**, 18, 4.
- [21] J. Fischer, M. Wegener, *Laser Photon. Rev.* **2012**, 7, 1.
- [22] E. Arzt, P. Fratzl, H. Gao, B. Ji, I. L. Ja, *Proc. Natl. Acad. Sci. USA* **2003**, 100, 10.
- [23] J. R. Greer, D. Jang, X. W. Gu, *JOM* **2012**, 64, 10.
- [24] L. J. Gibson, *J. Biomech.* **2005**, 38, 3.